Tuning Low-Spin to High-Spin Mn Pairs in 2-D ZnO by Injecting Holes

R. H. Miwa, T. M. Schmidt, and A. Fazzio

***Abstract*—We have performed an *ab initio* theoretical investigation of substitutional Mn_{Zn} atoms in planar structures of ZnO, *viz.*, monolayer [$(ZnO)_1$] and bilayer [$(ZnO)_2$] systems. Due to the 2-D quantum confinement effects, in those Mn -doped $(ZnO)_1$ and $(ZnO)_2$ structures, the antiferromagnetic (AFM) coupling between (nearest neighbor) Mn_{Zn} impurities have been strengthened when compared with the one in ZnO bulk systems. On the other hand, we find that the magnetic state of these systems can be tuned from AFM to FM by adding holes, which can be supplied by a p-type doping or even photoionization processes. Whereas, upon addition of electrons (n-type doping), the system keeps its AFM configuration.**

***Index Terms*—Nanotechnology, ZnO, spintronics.**

I. Introduction

ZNO EXHIBITS different structural phases, which can be tailored in a suitable way aiming different applications, *viz*., nanogenerators made of ZnO nanowires [1], and (most recently) organic–inorganic junctions composed by thin layers of polycrystalline ZnO [2]. Bulk ZnO presents the hexagonal wurtzite structure, $ABAB$ staking, with the Zn and O atoms lying at different planes along the [0001] direction. The vertical distance between these Zn and O layers is 0.63 Å. Meanwhile, recent experimental investigations verified the formation of graphitic thin films of ZnO, where (similar to h-BN) the Zn atoms lie approximately at the same plane of O atoms [3]. The formation of flat ZnO layers was observed through scanning tunneling microscopy images. They find flat surfaces for $\sim$2 monolayers (MLs) of ZnO. It is worth mentioning that the formation of graphitic ZnO phase (for few layers of ZnO) was proposed one year before by Freeman *et al*. [4], based upon *ab initio* total energy calculations.

In parallel to the possibility of design of new nanostructures, ZnO has been considered a promising material to build up magnetic semiconductor devices based on diluted magnetic semiconductors (DMS). For instance, ferromagnetism above room temperature in Mn-doped thin films of ZnO (2–3 μm thick and Mn concentration below 4 %) [5], and (very recently) intrinsic ferromagnetism in ZnO nanoparticles doped with Fe and Co [6]. Recent experimental studies indicate that defects like vacancies, and others related to the formation of grain boundaries, are important to the ferromagnetic (FM) coupling between the Mn–Mn impurity atoms [7], [8]. The role played by intrinsic defects and codopants on the ferromagnetism in Mn-doped ZnO has been the subject of numerous theoretical investigations, for instance, Zn and O vacancies [9], and codopants like N [10], Cu, and Li [11]. On the other hand, with no defects or codopants, Mn impurities in ZnO present an anti-FM (AFM) coupling [12], [13]. Theoretical studies, performed within the *ab initio* density functional theory (DFT), propose that the antiferromagnetism of Mn_{Zn} is ruled by a superexchange interaction between the Mn 3d orbitals, being mediated by the adjacent O 2p orbitals [12], [14]. Nowadays, there is a great effort in tailoring the magnetic and electronic properties of DMS, for instance,focusing on getting higher Curie temperatures through the inclusion of codopants and/or modifying the atomic structure of the host like in nanowires, nanoparticles, and thin films of ZnO.

In this paper, we perform a detailed theoretical DFT investigation of Mn-doped 2-D structures, i.e. monolayers [$(ZnO)_1$] and bilayers [$(ZnO)_2$] systems of ZnO. Initially, we examine the electronic and structural properties of pristine $(ZnO)_1$ and $(ZnO)_2$. Then, we next include substitutional Mn (impurity) atoms. For both systems, $(ZnO)_1$ and $(ZnO)_2$, we find that there is an energetic preference for Mn atoms lying on the nearest neighbor (NN) Zn sites, Mn_{Zn}. The energetic preference for the AFM or FM state can be measured by comparing the total energies of the AFM ($E_{\rm AFM}$) and FM ($E_{\rm FM}$) systems, $\Delta E_{\rm AFM-FM} = E_{\rm AFM} - E_{\rm FM}$. We find higher values of $\Delta E_{\rm AFM-FM}$, -0.21 and -0.13 eV for $(ZnO)_1$ and $(ZnO)_2$, respectively, in comparison with the one obtained in the ZnO bulk phase, thus, indicating that the AFM state has been strengthened in these 2-D systems of Mn-doped ZnO. Based upon our electronic band structure calculations, we inferred that the AFM state can be tuned to an FM state in the presence of holes. Indeed, we find FM couplings with $\Delta E_{\rm AFM-FM} = +0.16$ and $+0.31$ eV by adding a hole to the highest occupied $a1'$ level of the Mn_{Zn}-doped $(ZnO)_1$ and $(ZnO)_2$ systems, respectively.

II. Computational Details

Our calculations were performed within the DFT, as implemented in the Spanish Initiative for Electronic Simulations with

Manuscript received April 22, 2010; revised September 15, 2010; accepted April 18, 2011. Date of publication May 5, 2011; date of current version January 11, 2012. This work was supported by the Brazilian agencies Conselho Nacional de Desenvolvimento Científico e Tecnológico (CNPq), Fundação de Amparo à Pesquisa do Estado de Minas-Gerais (FAPEMIG), and Fundação de Amparo à Pesquisa do Estado de São Paulo (FAPESP), and by Centro Nacional de Processamento de Alto Desempenho de São Paulo (CENAPAD/SP). The review of this paper was arranged by Associate Editor J.-P. Leburton.

R. H. Miwa and T. M. Schmidt are with the Instituto de Física, Universidade Federal de Uberlândia, Uberlândia, Uberlândia, Minas Gerais 38400-902, Brazil (e-mail: hiroki@infis.ufu.br).

A. Fazzio is with the Instituto de Física, Universidade de São Paulo, São Paulo 38400-970, Brazil.

Color versions of one or more of the figures in this paper are available online at http://ieeexplore.ieee.org.

Digital Object Identifier 10.1109/TNANO.2011.2150760

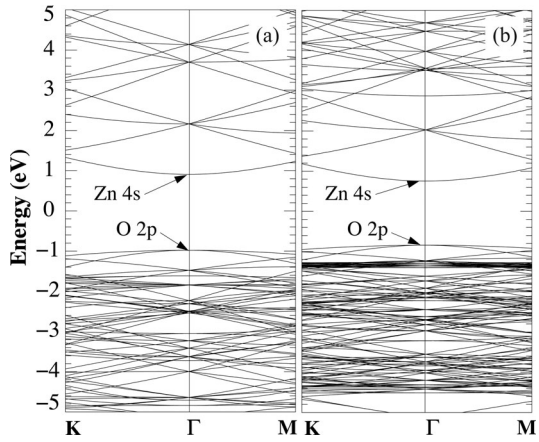

Fig. 1. Electronic band structure of pristine ZnO sheets, monolayer [$(ZnO)_1$] (a) and bilayer [$(ZnO)_2$] (b) systems.

Thousands of Atoms (SIESTA) code [15]. Local spin density approximation (LSDA) [16] approach has been used do calculate the exchange–correlation energy. The Kohn–Sham (KS) orbitals were described by linear combinations of numerical pseudoatomic orbitals using a split-valence double-zeta basis set including polarization functions [17]. The electron–ion interactions were calculated by using norm-conserving pseudopotentials [18]. All the atomic positions were relaxed by using the conjugated gradient scheme, within a force convergence criterion of 20 meV/Å. The ZnO sheets were describe within the supercell approach, using a 6×6 surface unit cell with 72 and 144 atoms for the $(ZnO)_1$ and $(ZnO)_2$ structures, respectively.

III. Results and Comments

Pristine ZnO monolayer and bilayer systems present semiconducting character, as depicted in the electronic band structures shown in Fig. 1(a) and (b), respectively. We find that the electronic band structure of $(ZnO)_1$ and $(ZnO)_2$ are very similar, with energy bandgaps of 1.89 and 1.60 eV, respectively. Within the same LSDA, for the ZnO bulk system, we obtained a bandgap of 0.90 eV. For both systems, the highest occupied and lowest unoccupied states mostly come from O 2p and Zn 4s orbitals, respectively. At the equilibrium geometry, the $(ZnO)_1$ exhibits a planar structure, where the Zn and O atoms are at the same plane with Zn–O bond length ($d_{\mathrm{Zn-O}}$) of 1.87 Å. In contrast, for $(ZnO)_2$, there is a slight vertical buckling of 0.07 Å between Zn and O atoms. The Zn–O bond length is stretched by 0.06 Å ($d_{\mathrm{Zn-O}} = 1.93$ Å) compared with the monolayer structure, and the vertical distance between the ZnO monolayer is 2.22 Å. These equilibrium geometry results are in good agreement with the recent experimental X-ray diffraction measurements [3].

We next examined the equilibrium geometry of a substitutional Mn atom occupying a Zn site in the $(ZnO)_1$ sheet, $Mn_{Zn}/(ZnO)_1$. Initially, we considered symmetric relaxations of the (three planar) Mn–O bonds in order to keep the D_{3h} symmetry. The planar structure has been maintained, and we find Mn–O bond length ($d_{\mathrm{Mn-O}}$) of 1.91 Å. In accordance with the imposed D_{3h} symmetry, we find two doubly degenerated

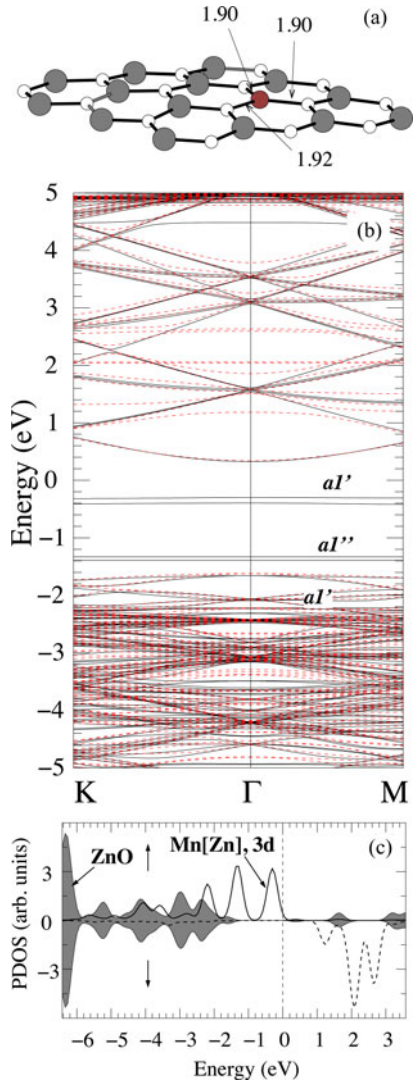

Fig. 2. (a) Structural model, (b) electronic band structure, and (c) projected density of states (PDOS) of the Mn_{Zn}-doped $(ZnO)_1$ sheet [$Mn_{Zn}/(ZnO)_1$]. In (a), the atomic distances are in angstrom, and in (b), solid (black) and dashed (red) lines represent the spin-up and spin-down electronic bands, respectively. In (c), solid (dashed) line represents the spin-up (spin-down) PDOS of Mn_{Zn} 3d orbital, and the shaded region indicates the PDOS of the ZnO host.

levels e' (composed by $3d_{xy}$ and $3d_{x^2-y^2}$ orbitals) and e'' ($3d_{xz}$ and $3d_{yz}$ orbitals) lying at 0.32 and 1.35 eV below the Fermi level, respectively. These e' and e'' levels are localized within the $(ZnO)_1$ bandgap, whereas the single occupied a_1 level ($3dz^2$) is resonant within the valence band, 2.23 eV below the Fermi level. The Mn–O bond length is slightly larger than $d_{\mathrm{Zn-O}}$, and thus, the Zn–O bonds are compressed nearby Mn_{Zn}. Removing the imposed symmetry constraint, there is an upward displacement of 0.59 Å of the Mn_{Zn} substitutional atom, and we obtain $d_{\mathrm{Mn-O}}$ equilibrium bond lengths of 1.90 and 1.92 Å, as depicted in Fig. 2(a). The calculated total energy reduces by 60 meV. In this case, the $Mn_{Zn}/(ZnO)_1$ structure exhibits a C_s symmetry and there is an energy splitting of the occupied e' and e'' levels of 0.10 ($a1' + a1'$) and 0.06 eV ($a1'' + a1''$), respectively, as shown in Fig. 2(b). The occupied Mn 3d orbitals, lying within an energy interval of 3 eV below the Fermi

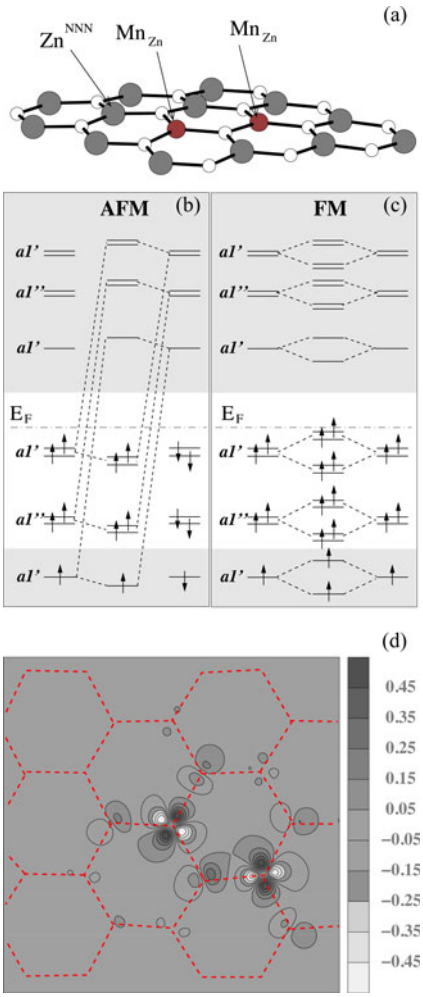

Fig. 3. (a) Structural model and schematic representation of the energy levels for (b) AFM and (c) FM states of $Mn(2)_{Zn(2)}/(ZnO)_1$ sheet. Spatial distribution, in $(au)^{-3/2}$, of the Mn $3d_{x^2-y^2}$, $3d_{xy}$, and O 2p orbitals (at the Γ point).

level [see Fig. 2(c)], give rise to a net magnetization of 4.94 μ_B for the $Mn_{Zn}/(ZnO)_1$ system. The dispersionless character of Mn_{Zn}-induced states, within the $(ZnO)_1$ band structure, is in accordance with the very localized character of those Mn 3d orbitals. Similar flat energy bands have been verified for NN Mn_{Zn} pairs in $(ZnO)_1$ and $(ZnO)_2$ sheet systems.

For the second substitutional Mn_{Zn} atom in the $(ZnO)_1$ sheet, which corresponds to a Mn concentration of 2.8%, we find that there is an energetic preference for two Mn_{Zn} occupying the NN Zn sites, $Mn(2)_{Zn(2)}/(ZnO)_1$ [see Fig. 3(a)]. For instance, Mn_{Zn} in the next NN site (NNN), Zn^{NNN} in Fig. 3(a), is energetically less favorable by 0.19 eV. Comparing the total energies for the AFM and FM coupling between the two NN Mn_{Zn} (ΔE_{AFM-FM}), we find that the AFM system represents the ground state configuration by 0.21 eV ($\Delta E_{AFM-FM} = -0.21$ eV). Whereas for $Mn(2)_{Zn(2)}$ in ZnO bulk, the AFM state is more stable by 0.07 eV, $\Delta E_{AFM-FM} = -0.07$ eV. We can infer that the increase of the superexchange splitting in $Mn(2)_{Zn(2)}/(ZnO)_1$ comes from the quantum confinement effects of the 2-D $(ZnO)_1$ host. The energetic preference for the AFM configuration is in accordance with the recently proposed phenomenological band structure models for magnetic couplings in semiconductors [12], [14]. Fig. 3(b) indicates that the superexchange interaction between the spin-up (occupied) majority and (unoccupied) minority $a1$ states of Mn 3d orbitals, mediated by the adjacent O 2p orbitals, rules the AFM coupling in $Mn(2)_{Zn(2)}/(ZnO)_1$. Although the AFM coupling has been strengthened in ZnO sheet systems, due to the very localized character of the Mn 3d orbitals, the exchange interactions become negligible for Mn_{Zn} atoms occupying NNN Zn sites ($\Delta E_{AFM-FM} = -0.6$ meV).

In this case, the highest occupied $a1'$ state moves downward by $\sim$0.05 eV, while $a1''$ ($3d_{xz}$ and $3d_{yz}$) and $a1'$ ($3d_{z^2}$) levels suffer negligible perturbations due to the Mn_{Zn}–Mn_{Zn} interaction. We will have same picture for the spin-down orbitals (not shown). On the other hand, for the FM coupling [see Fig. 3(c)], we observe that there is no net energy gain upon the electronic exchange interactions between the occupied Mn_{Zn} 3d states [19]. At the equilibrium geometry, as a consequence of the Pauli exclusion principle, the Mn_{Zn}–Mn_{Zn} distance (d_{Mn-Mn}) is slightly larger for the FM state, namely, we obtained d_{Mn-Mn} of 3.27 and 3.30 Å for the AFM and FM states, respectively. In order to verify the role played by the ZnO host, we calculate the exchange energy for an isolated Mn dimer, however, keeping the Mn–Mn bond distances as the ones obtained in the $(ZnO)_1$ host, namely, 3.27 (AFM) and 3.30 Å (FM). In this case, we obtained $\Delta E_{AFM-FM} = -0.03$ eV, indicating that indeed the presence of $(ZnO)_1$ host is quite important for the AFM coupling between NN Mn_{Zn} atoms. Fig. 3(d) presents the spatial distribution of the electronic wave function of the highest occupied $a1'$ level, composed by $3d_{x^2-y^2}$ and $3d_{xy}$ orbitals from the NN Mn_{Zn} atoms and the adjacent O 2p orbital, supporting the superexchange picture for the AFM coupling in the $Mn(2)_{Zn(2)}/(ZnO)_1$ system.

Since the AFM and FM systems exhibit different equilibrium geometries, for instance, the Mn_{Zn}–Mn_{Zn} distances, it is interesting to somewhat separate the exchange contribution from our total energy results. Keeping the equilibrium geometries as those obtained for the AFM and FM systems, we perform nonspin-polarized calculations of the $Mn(2)_{Zn(2)}/(ZnO)_1$ system, i. e., the spin coordinate is (artificially) suppressed. We find that AFM equilibrium atomic geometry is energetically more stable by 0.04 eV in comparison with the FM equilibrium geometry, i.e., for Mn_{Zn}–Mn_{Zn} distance of 3.27 Å (AFM geometry), the strain induced in the $(ZnO)_1$ lattice is lower compared with the one for Mn_{Zn}–Mn_{Zn} distance of 3.30 Å (FM geometry). Thus, comparing with our calculated exchange energy ($\Delta E_{AFM-FM} = -0.21$ eV), we can estimate that the rest of ΔE_{AFM-FM}, -0.17eV, comes from the (net) exchange interactions between the Mn 3d levels once the spin degree of freedom is turned on.

Fig. 4(a) presents the equilibrium atomic structure of a single substitutional Mn_{Zn} atom in the ZnO bilayer system, $Mn_{Zn}/(ZnO)_2$. Comparing the calculated formation energies, we find that 1) the energy cost to the formation of substitutional Mn_{Zn} in $(ZnO)_2$ is lower by 0.13 eV when compared to Mn_{Zn} in $(ZnO)_1$, and 2) the formation energy of $Mn_{Zn}/(ZnO)_2$ is the

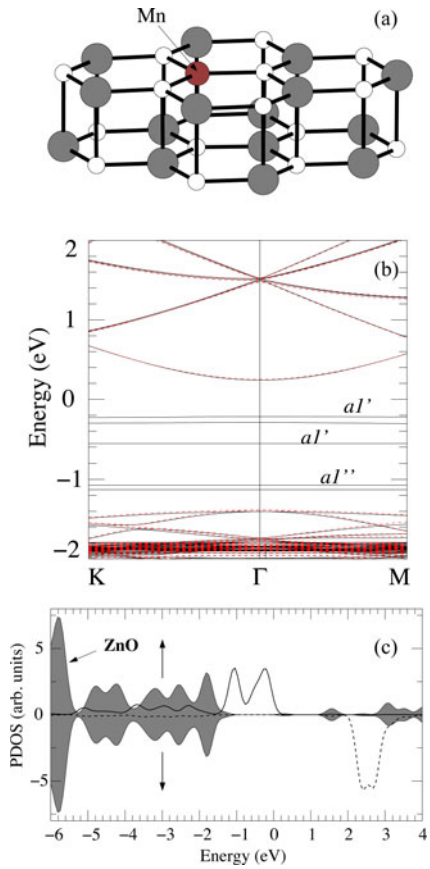

Fig. 4. (a) Structural model, (b) electronic band structure, and (b) projected density of states (PDOS) of the Mn_{Zn}-doped $(ZnO)_2$ sheet [$Mn_{Zn}/(ZnO)_2$]. In (b), solid (black) and dashed (red) lines represent the spin-up and spin-down electronic bands, respectively. In the PDOS diagram, solid (dashed) line represents the spin-up (spin-down) PDOS of Mn_{Zn} 3d orbital, and the shaded region indicates the PDOS of the ZnO host .

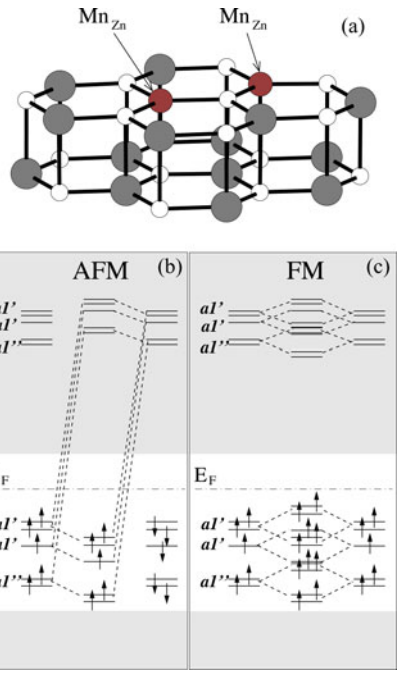

Fig. 5. (a) Structural model and schematic representation of the energy levels for (b) AFM and (c) FM states of $Mn(2)_{Zn(2)}/(ZnO)_2$ sheet.

same as that obtained for Mn_{Zn} in ZnO bulk. At the equilibrium geometry, the Mn_{Zn} atom is fourfold coordinated, with Mn–O bond lengths of 1.94 and 1.96 Å (2.23 Å) parallel (perpendicular) to the $(ZnO)_2$ surface. The C_s symmetry has been maintained, where the $a1'$ and $a1''$ levels lie within the energy bandgap [see Fig. 4(b)]. For two Mn_{Zn} impurities, $Mn(2)_{Zn(2)}/(ZnO)_2$ [see Fig. 5(a)], the AFM state represents the ground state configuration, $\Delta E_{AFM-FM} = -0.13$ eV. This is mainly ruled by superexchange interactions between the Mn_{Zn} 3d $a1$ states [see Fig. 5(b)]. Whereas, similar to the $Mn(2)_{Zn(2)}/(ZnO)_1$ system, there is no energy gain for the FM state, as shown in Fig. 5(c). The calculated single-particle KS eigenvalues allow us to get a picture of the electronic interactions between the $a1$ levels for the AFM system. We find that most of the energetic stability of the AFM state comes from the repulsive interactions between the occupied and the unoccupied $a1'$ levels composed by Mn_{Zn} $3d_{xy}$ and $3d_{x^2-y^2}$ orbitals.

Turning off the spin coordinate, however, keeping the equilibrium geometries obtained for the AFM and FM structures, we find that the latter system (Mn–Mn distance of 3.22 Å) is energetically more stable by 0.07 eV when compared with the one with Mn–Mn distance of 3.18 Å (AFM geometry). Thus, the superexchange interaction should overcome this total energy difference (of 0.07 eV) in order to stabilize the AFM state on $Mn(2)_{Zn(2)}/(ZnO)_2$. In this case, we can roughly estimate an electronic contribution of 0.20 eV for the superexchange splitting that stabilizes the AFM state in $Mn(2)_{Zn(2)}/(ZnO)_2$, which is quite comparable with the one obtained in the $Mn(2)_{Zn(2)}/(ZnO)_1$ system, 0.17 eV.

The electronic levels depicted in Figs. 3 and 5 suggest that it is possible to get FM $Mn(2)_{Zn(2)}/(ZnO)_1$ and $Mn(2)_{Zn(2)}/(ZnO)_2$ structures through ionization processes. In those systems, the AFM and FM states are ruled by the energy coupling between the Mn_{Zn} 3d orbitals, which can be measured by the superexchange ($\Delta^{1,2}_{dd}$) and direct-exchange (Δ^{1}_{dd}) parameters [14], [20]. In particular, for $Mn(2)_{Zn(2)}/(ZnO)_1$ and $Mn(2)_{Zn(2)}/(ZnO)_2$, $\Delta^{1,2}_{dd}$ represents the repulsive interaction between the majority and minority spin states, where the occupied (majority) and unoccupied (minority) states are separated by an exchange splitting (ε_{dd}) of ~3.0 eV (for the $3d_{xy}$ and $3d_{x^2-y^2}$ orbitals) and ~3.4 eV (for the $3d_{xz}$, $3d_{yz}$, and $3d_{z^2}$ orbitals). Δ^{1}_{dd} represents the energy splitting between the occupied majority spin states and between the unoccupied minority spin states. Since in Δ^{1}_{dd} we have no exchange splitting between the coupled states, $\varepsilon_{dd} = 0$, it is expected that $\Delta^{1}_{dd} > \Delta^{1,2}_{dd}$ [14].

From Figs. 3 and 5, we verify that to create a hole, we have to remove a single electron from the highest occupied $a1'$ level. This hole can be supplied by a p-type doping or even photoionization processes. Within our supercell approach, by removing a single electron, we will have a hole concentration of around 10^{13} cm^2. In this case, compared with the neutral systems, the energy gain for the AFM state will be reduced by $\Delta^{1,2}_{dd}$, while we will have a net energy gain of Δ^{1}_{dd} for the FM state. Indeed, our total energy results indicate

that $Mn(2)_{Zn(2)}/(ZnO)_1$ and $Mn(2)_{Zn(2)}/(ZnO)_2$ become FM by adding a hole. We find $\Delta E_{AFM-FM} = +0.16$ and $+0.31$ eV for the $Mn(2)_{Zn(2)}/(ZnO)_1$ and $Mn(2)_{Zn(2)}/(ZnO)_2$ systems, respectively. Since for the FM states we are removing an electron from the antibonding Mn_{Zn} 3d orbital, there is a slight reduction on the Mn–Mn distance compared with the neutral systems, *viz*., $3.30 \rightarrow 3.29$ Å and $3.22 \rightarrow 3.19$ Å for FM $Mn(2)_{Zn(2)}/(ZnO)_1$ and $Mn(2)_{Zn(2)}/(ZnO)_2$ structures, respectively. In contrast, the AFM state has been maintained by adding an electron (n-type doping). In this case, the superexchange splittings are almost the same as the ones obtained for the neutral systems, namely, for the negatively charged (neutral) systems, we find $\Delta E_{AFM-FM} = -0.22$ (-0.21) and -0.16 eV (-0.13 eV). This is in accordance with the energy position of the KS eigenvalues obtained within our LSDA calculations. The lowest unoccupied Mn_{Zn} 3d orbitals are resonant within the conduction band, lying at 0.9 [$Mn(2)_{Zn(2)}/(ZnO)_1$] and 2.1 eV [$Mn(2)_{Zn(2)}/(ZnO)_2$] above the conduction band. Thus, most of the additional electron will be delocalized within the conduction band of the ZnO host.

It is worth to address here a comment regarding the underestimation of the calculated energy band gaps, as compared with experimental ones, and its consequence on the results presented in this paper. Its well known that the energy gaps are underestimated within the standard DFT-local density approximation (LDA) approach. However, we recently showed that this reduction of the calculated energy gaps for Co-doped confined systems, like ZnO sheets, does not lead to wrong occupancy [23]. Indeed, there are several theoretical studies addressing the importance of an accurate description of the energy gap in FM versus AFM coupling in Co-doped ZnO bulk [20]–[22], and more recently, a general analysis has been presented for DMS, showing when the theory fails due to false occupancy [24]. In low-dimensional ZnO sheets, the energy bandgap increases in comparison with the bulk system. In particular, the magnetic properties of Co-doped ZnO monolayer systems are well described through standard DFT-LDA approach [23]. Here, the AFM configuration for the neutral, and the FM configuration for the positively charged $Mn(2)_{Zn(2)}/(ZnO)_1$ and $Mn(2)_{Zn(2)}/(ZnO)_2$ systems will not change upon an accurate description of the energy bandgap. Whereas for the negatively charged system, we may face a different picture if the empty Mn 3d states were placed inside the bandgap, *viz*., the $Mn(2)_{Zn(2)}/(ZnO)_1$ and $Mn(2)_{Zn(2)}/(ZnO)_2$ systems will also become FM by adding electrons.

IV. Summary

In summary, we have examined in detail the electronic and magnetic properties of Mn-doped 2-D structures of ZnO. Similarly to the ZnO bulk, at the ground state, the NN Mn_{Zn} impurities embedded in planar $(ZnO)_1$ and $(ZnO)_2$ sheets also present AFM couplings. However, due to the 2-D quantum confinement effects, the energetic preference for the AFM state has been strengthened in those ZnO planar hosts. Based upon our total energy results, we find ΔE_{AFM-FM} of -0.21 and -0.13 eV for $Mn(2)_{Zn(2)}/(ZnO)_1$ and $Mn(2)_{Zn(2)}/(ZnO)_2$ systems, respectively. Further electronic band structure calculations indicate that the AFM state can be tuned to FM state by adding holes (through p-type doping or photoionization processes). Indeed, for the positively charged $Mn(2)_{Zn(2)}/(ZnO)_1$ and $Mn(2)_{Zn(2)}/(ZnO)_2$ systems, we find $\Delta E_{AFM-FM} = +0.16$ and $+31$ eV, respectively. These results allow us to infer that the FM state should be stable even at high temperature, particularly for $Mn(2)_{Zn(2)}/(ZnO)_2$. In contrast, the AFM state has been kept for the negatively charged systems. In this case, our calculated electronic band structure indicates that the additional electron will spread out in the conduction band of the ZnO host.

References

[1] Z. L.Wang, S. J. Song, "Piezoelectric nanogenerators based on zinc oxide nanowire arrays," *Science*, vol. 312, pp. 242–246, Apr. 2006.

[2] M. Sofos, J. Goldberg, D. A. Stone, J. E. Allen, Q. Ma, D. J. Herman, W. W. Tsai, L. J. Lauhon, and S. I. Stupp, "A synergistic assembly of nanoscale lamellar photoconductor hybrids," *Nat. Mater.*, vol. 8, pp. 68–75, Jan. 2008.

[3] C. Tusche, H. L. Meyerheim, and J. Kirschner, "Observation of depolarized ZnO(0001) monolayers: Formation of unreconstructed planar sheets," *Phys. Rev. Lett.*, vol. 99, pp. 026102-1–026102-4, Jul. 2007.

[4] C. L. Freeman, F. Claeyssens, and N. L. Allan, "Graphitic nanofilms as precursors to wurtzite films: Theory," *Phys. Rev. Lett.*, vol. 96, pp. 066102-1–066102-4, 2006.

[5] P. Sharma, A. Gupta, K. V. Rao, F. J. Owens, R. Sharma, R. Ahuja, J. M. Osorio, B. Johansson, and G. Gehring, "Ferromagnetism above room temperature in bulk and transparent thin films of Mn-doped ZnO," *Nat. Mater.*, vol. 3, pp. 673–677, Dec. 2003.

[6] Z. H. Zhang, X. Wang, J. B. Xu, S. Muller, C. Ronning, and Q. Li, "Evidence of intrinsic ferromagnetism in individual dilute magnetic semiconducting nanostructures," *Nat. Nanotechnol.*, vol. 4, pp. 523–527, Aug. 2009.

[7] B. B Straumal, A. Mazilkin, S. Protasova, A. Myatiev, P. Straumal, G. Schütz, P. van Aken, and B. Baretzky, "Magnetization study of nanograined pure and Mn-doped ZnO films: Formation of a ferromagnetic grain-boundary foam," *Phys. Rev. B*, vol. 79, pp. 205206-1–205206-7, May 2009.

[8] M. Kapilashrami, J. Xu, V. Ström, K. Rao, and L. Belova, "Transition from ferromagnetism to diamagnetism in undoped ZnO thin films," *Appl. Phys. Lett.*, vol. 95, pp. 033104-1–033104-3, Jul. 2009.

[9] D. Iusan, B. Sanyal, and O. Eriksson, "Theoretical study of the magnetism of Mn-doped ZnO with and without defects," *Phys. Rev. B*, vol. 74, pp. 235208-1–235208-8, Dec. 2006.

[10] H. L. Yan, X. L. Zhong, J. Wang, G. Huang, S. Ding, G. Zhou, and Y. Zhou, "Cathodoluminescence and room temperature ferromagnetism of Mn-doped ZnO nanorod arrays grown by chemical vapor deposition," *Appl. Phys. Lett.*, vol. 90, pp. 082503-1–082503-3, Feb. 2007.

[11] Y. Zhu, J. X. Cao, Z. Q. Yang, and R. Q. Wu, "Origin of the codopant-induced enhancement of ferromagnetism in (Zn,Mn)O: Density functional calculations," *Phys. Rev. B*, vol. 79, pp. 085206-1–085206-5, Feb. 2009.

[12] M. H. Sluiter, Y. Kawazoe, P. Sharma, A. Inoue, A. R. Raju, C. Rout, and U. V. Waghmare, "First principles based design and experimental evidence for a ZnO-based ferromagnet at room temperature," *Phys. Rev. Lett.*, vol. 94, pp. 187204-1–187204-4, May 2005.

[13] T. Chanier, F. Virot, and R. Hayn, "Chemical trend of exchange coupling in diluted magnetic II-VI semiconductors: Ab initio calculations," *Phys. Rev. B*, vol. 79, pp. 205204-1–205204-8, May 2009.

[14] G. M. Dalpian, S.-H. Wei, X. Gong, A. J. da Silva, and A. Fazzio, "Phenomenological band structure model of magnetic coupling in semiconductors," *Sol. State Comm.*, vol. 138, pp. 353–358, Mar. 2006.

[15] J. M. Soler, E. Artacho, J. D. Gale, A. García, J. Junquera, P. Ordejón, and D. Sánchez-Portal, "The SIESTA method for ab initio order-N materials simulation," *J. Phys.: Condens. Matter*, vol. 14, pp. 2745–2779, Mar. 2002.

[16] D. M. Ceperley and B. J. Alder, "Ground state of the electron-gas by a stochastic method," *Phys. Rev. Lett.*, vol. 45, pp. 566–569, Aug. 1980.

[17] Within the SIESTA code, the cutoff radius of the basis set (pseudoatomic orbitals) can be tuned by a single parameter, *energy shift*. For lower *energy*

shift we have larger cutoff radii for the atomic orbitals, that is, the basis set has been improved. In the present work we have considered an energy shift of 0.10 eV to determine the radius cutoff of the pseudoatomic orbitals. In addition, we verify the convergence of our total energy results for lower *energy shift*, 0.05 eV.

[18] N. Troullier and J. L. Martins, "Efficient pseudopotentials for plane-wave calculations," *Phys. Rev. B*, vol. 43, pp. 1993–2006, Jan. 1991.

[19] Here we are considering only the orbital couplings between the Mn_{Zn} 3d states, since there is no net energy gain upon the interaction between the Mn 3d and the host e' states, composed by O 2p orbitals, of the valence band maximum.

[20] A. Walsh, J. L. L. D. Silva, and S.-H. Wei, "Theoretical description of carrier mediated magnetism in cobalt doped ZnO," *Phys. Rev. Lett.*, vol. 100, pp. 256401-1–256401-4, Jun. 2008.

[21] C. D. Pemmaraju, R. Hanafin, T. Archer, H. B. Braun, and S. Sanvito, "Impurity-ion pair induced high-temperature ferromagnetism in Co-doped ZnO," *J. Phys. Rev. B*, vol. 78, pp. 054428-1–054428-10, Aug. 2008.

[22] S. Lany, H. Raebiger, and A. Zunger, "Magnetic interactions of Cr-Cr and Co-Co impurity pairs in ZnO within a band-gap corrected density functional approach," *Phys. Rev. B*, vol. 77, pp. 241201-1–241201-4, Jun. 2008.

[23] T. M. Schmidt, R. H. Miwa, and A. Fazzio, "Ferromagnetic coupling in a Co-doped graphene like ZnO sheet," *Phys. Rev. B*, vol. 81, pp. 195413-1–195413-4, May 2010.

[24] A. Zunger, S. Lany, and H. Raebiger, "The quest for dilute ferromagnetism insemiconductors: Guides and misguides by theory," *Physics*, vol. 3, p. 53, Jun. 2010.

Author's photographs and biographies not available at the time of publication.